DRAFT VERSION JULY 15, 2013
Preprint typeset using LaTeX style emulateapj v. 11/10/09

MODEL FITTING BIAS DUE TO SED-DEPENDENT PSFS

J. MEYERS[1], THE AUTHORS

Draft version July 15, 2013

ABSTRACT

This is the abstract.

1. INTRODUCTION

Cosmic shear experiments aim to constrain cosmological parameters by measuring the small departure from statistical isotropy of distant galaxy shapes induced by the gravitational lensing from foreground large scale structure. The shapes of galaxy images collected from telescopes, however, are not only affected by cosmic shear (typically a $\sim 1\%$ effect), but also by the combined point spread function (PSF) of the atmosphere (for ground-based experiments), telescope optics, and the image sensor (often a few % effect). The shape of this additional convolution kernel is typically constrained from the shapes of stars, which are effectively point sources before being smeared by the PSF. Galaxy images can then be deconvolved with the estimated convolution kernel. Implicit in this approach is the assumption that the galactic kernel is the same as the stellar kernel. Effects that make the PSF dependent on wavelength will violate this assumption, as stars and galaxies at different redshifts, have different spectral energy distributions, and hence different PSFs.

Examples of wavelength-dependent PSF contributions include:

- atmospheric differential chromatic refraction (DCR)
- atmospheric seeing
- telescope optics DCR
- photoconversion depth in the sensor and subsequent charge diffusion

This note will focus on PSF mis-estimations due to the first of the above effects, though the conclusions are applicable to any situation in which the bias due to using the wrong PSF is estimated using a ring test with a simple model parameterization.

2. ANALYTIC EXPECTATIONS

Plazas & Bernstein (2012) derived analytic expressions for the bias expected in weak lensing measurements due to differential chromatic refraction. We summarize the main points of their argument here.

Let $R(\lambda, z_a)$ be the refraction towards the zenith of a photon with wavelength λ and true zenith angle (before refraction) z_A. The refraction can be factored into

$$R(\lambda; z_a) = g(\lambda)\tan(z_a) \tag{1}$$

and $g(\lambda)$, which implicitly depends on air pressure, temperature, and the partial pressure of water vapor, and can be obtained from Edlen (1953) and Coleman et al. (1960). For monochromatic sources, the only effect is to move the apparent position of the object. For sources which are not monochromatic (i.e. all real sources), having a wavelength density of surviving photons (i.e. the product of the source photon density and the total system throughput function) given by $\mathrm{p}_\lambda(\lambda)$, the mismatched displacements of different wavelengths introduces a convolution kernel in the zenith direction that can be written in terms of the inverse of Equation 1:

$$h(R) = \frac{p_\lambda(\lambda(R; z_a))\left|\frac{\mathrm{d}\lambda}{\mathrm{d}R}\right|}{\int p_\lambda(\lambda)\,\mathrm{d}\lambda} \tag{2}$$

This kernel can largely be characterized in terms of its first and second central moments given by:

$$\bar{R} = \int h(R) R\,\mathrm{d}R = \frac{\int R(\lambda; z_a) p_\lambda(\lambda)\,\mathrm{d}\lambda}{\int p_\lambda(\lambda)\,\mathrm{d}\lambda} \tag{3}$$

$$V = \int h(R)(R-\bar{R})^2\,\mathrm{d}R = \frac{\int (R(\lambda; z_a)-\bar{R})^2 p_\lambda(\lambda)\,\mathrm{d}\lambda}{\int p_\lambda(\lambda)\,\mathrm{d}\lambda} \tag{4}$$

Galaxy shapes can be characterized by the quadrupole moments of their light distribution given by:

$$I_{\mu\nu} = \frac{1}{f}\int \mathrm{d}x\,\mathrm{d}y I(x,y)\mu - \bar{\mu}(\nu - \bar{\nu}) \tag{5}$$

$$\bar{\mu} = \frac{1}{f}\int \mathrm{d}x\,\mathrm{d}y I(x,y)\mu \tag{6}$$

$$f = \int \mathrm{d}x\,\mathrm{d}y I(x,y) \tag{7}$$

In particular, galaxy size and 2-component ellipticity are frequently defined as:

$$r^2 = I_{xx} + I_{yy} \tag{8}$$

$$e_1 = \frac{I_{xx} - I_{yy}}{r^2} \tag{9}$$

$$e_2 = \frac{2I_{xy}}{r^2} \tag{10}$$

For the case of differential chromatic refraction, we can set, without loss of generality, the x direction to be towards zenith. The effect of DCR is then to take $I_{xx} \to I_{xx} + V$, which also takes $r^2 \to r^2 + V$, but leaves I_{yy} and I_{xy} unchanged. The ellipticity and size parameterizations are defined in terms of the quadrupole moments before the galaxy light distribution is smeared by the PSF, but we only have access to the light distribution after convolution. The second moments before (I^g) and after (I^o) convolution are related via the second moments

jmeyers3@stanford.edu
[1] Department of Physics, Stanford University, Stanford, CA 94305

of the PSF (I^*) like $I^g = I^o - I^*$. If the SEDs of galaxies and stars were the same, then the effect of DCR would be to add V to both I^o and I^*, which would then cancel when computing I^g and subsequently galaxy shape parameters. The differences between stellar and galactic SEDs, however, will introduce a small error $\Delta V \ll r^2$ into I_{xx} and r^2, which leads to biases in the derived ellipticity parameters:

$$e_1 \rightarrow \frac{I_{xx} + I_{yy} + \Delta V}{r^2 + \Delta V} \approx e_1 \left(1 + \frac{\Delta V}{r^2}\right) + \frac{\Delta V}{r^2} \quad (11)$$

$$e_2 \rightarrow \frac{2I_{xy}}{r^2 + \Delta V} \approx e_2 \left(1 + \frac{\Delta V}{r^2}\right) \quad (12)$$

Under the expectation that $\langle e_i \rangle \approx 2\gamma_i$ and defining the shear calibration parameters m and c such that $\hat{\gamma} = \gamma(1 + m) + c$, where $\hat{\gamma}$ indicates the estimator for the true shear γ, we reach the expectation that $m = \frac{\Delta V}{r^2}$, $c_1 = m/2$, and $c_2 = 0$. Note that nowhere in the above analysis is there any assumption on the profile of the galaxy in question.

3. RING TEST

An alternative way to estimate the bias in $\hat{\gamma}$ induced by DCR is to simulate galaxy images using the "true" (galactic) PSF and then attempt to recover the simulated galactic ellipticities while pretending that the PSF is "wrong" (stellar). A ring test (Nakajima & Bernstein 2007) is a specific prescription for such a suite of simulations designed to rapidly converge to the correct value of $\hat{\gamma}$. The test gets its name from the arrangement of galaxy shapes used in the simulated images, which form a ring in ellipticity space (i.e. constant $|e|$), before any shear is applied. By choosing intrinsic ellipticities that exactly average to zero, the results of the test converge faster than for randomly (but isotropically) chosen ellipticities that only average to zero statistically.

The general procedure can be implemented as follows:

1. Choose an input "true" reduced shear g
2. Choose a pre-sheared ellipticity $e^s = (e_1^s, e_2^s)$
3. Compute the sheared ellipticity from $e^o = \frac{e^s + g}{1 + g^* e^s}$
4. Generate a "truth" image by convolving the galaxy model with the "true" PSF (galactic in this case)
5. Using a "reconstruction" PSF (stellar in this case), find the best fitting model to the "truth" image, record the measured ellipticity from the model parameters
6. Repeat steps 3-5 using the opposite pre-sheared ellipticity $-e^s$
7. Repeat steps 2-6 for as many values around the ellipticity ring as desired
8. Average all recorded output ellipticity values. This is the shear estimate $\hat{g}$
9. Repeat steps 1-8 to map out the relation $g(\hat{g})$
10. m and c are the slope and intercept of the best-fit linear relation between g and $\hat{g}$ (note we assume that $g \approx \gamma$)

As described above, the ring test requires some prescription for creating galaxy images with a given ellipticity. Here we investigate using a single Sersic profile as the galaxy model. The Sersic profile has 7 parameters: the x and y coordinates of the center, the total flux, the effective radius r_e (also called the half-light radius), the two component ellipticity $\mathbf{e}$, and the Sersic index n. Using r as an elliptical radial coordinate, the profile shape is:

$$I(r) \propto \mathrm{e}^{[-k(r/r_e)^2]^{\frac{1}{2n}}} \quad (13)$$

The constant $k \approx 1.9992n - 0.3271$ is chosen such that r_e is the half-light radius for a circularized profile. Limiting cases of the Sersic profile include the Gaussian profile which has $n = 0.5$, an exponential profile which has $n = 1.0$, and a de Vaucouleurs profile which has $n = 4.0$. The profile ranges from smoothly peaked with small tails at low n (such as an $n = 0.5$ Gaussian), to very sharply peak with heavy tails (such as an $n = 4.0$ deVaucoulers profile).

In addition to a galaxy model, the ring test also requires a model for the PSF. We have described above the PSF kernel that describes the contribution of DCR, but other contributions to the PSF also exist, due to atmospheric turbulence, telescope optics, and the detector for example. Ground based telescope PSFs are usually dominated by atmospheric turbulence, and are frequently modeled by a Moffat profile:

$$I_p(r) \propto \left(1 + \left(\frac{r}{\alpha}\right)^2\right)^{-\beta} \quad (14)$$

$$\alpha = \frac{\mathrm{FWHM}}{2\sqrt{2^{1/\beta} - 1}} \quad (15)$$

The PSF used in the ring test in this note is based on a Moffat profile with a FWHM of $0\farcs7$ and softening parameter $\beta = 2.6$. This base PSF is then convolved (in the zenith direction only) with the DCR kernel given in Equation 2. The "true" PSF uses a DCR kernel derived from a galaxy SED, while the "reconstruction" PSF uses a DCR kernel derived from a stellar SED.

4. SERSIC INDEX DEPENDENCE

The results of the ring test for set of Sersic galaxies are shown in Figure 1. The galaxy size quantified by r^2 is the same for each Sersic index. The ring test results match the analytic formulae well when Gaussian galaxies ($n = 0.5$) are used, but diverge by factors of 2-3 when de Vaucouleurs profiles ($n = 4.0$) are used. The PB12 analytic formalism has no dependence on the profile of the galaxy, but only on the assumption that the differential dispersion kernel is much smaller than the size of the unsmeared galaxy ($\Delta V \ll r^2$). This condition is met identically for each profile by construction, suggesting either that something is flawed with the PB12 formalism or with the ring test.

5. RING TEST CASE STUDY

To investigate the ring test in more detail, we have conducted a case study focusing on the redshift 1.25 galaxy that shows the largest m and c values in both the ring test results and the PB12 results. For this study, we have constructed a series of diagnostic images showing the results of the fits in Step 5 of the ring test for each of the Sersic indices studied. These diagnostic images are shown in Figures 2, 3, and 4. Note that

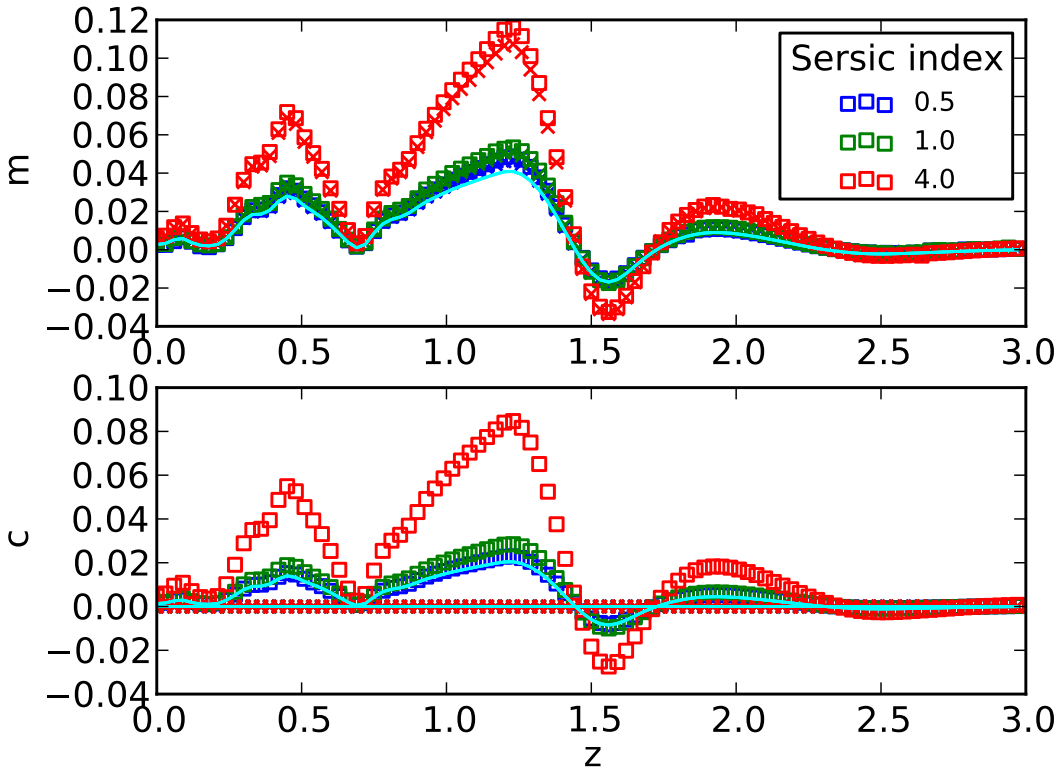

FIG. 1.— The shear calibration parameters m and c plotted against redshift. The results are obtained from the ring test assuming a true PSF derived from an elliptical galaxy spectrum and reconstruction PSF derived from a G5v stellar spectrum. The true galaxy images are simulated using the values: $r_e = 1.1$, and $|g| = 0.2$. Three values of the galaxy Sersic parameter n are shown: $n = 0.5$, corresponding to a Gaussian profile (blue), $n = 1.0$, corresponding to an exponential profile (green), and $n = 4.0$, corresponding to a de Vaucouleurs profile (red). The cyan line in each panel shows the analytic result from the PB12 formalism. The zenith angle is 30 degrees.

the diagnostic figures were generated for a zenith angle of 60 degrees for better visualization, though the qualitative results are the same at 30 degrees.

In Figures 2, 3, and 4, the "truth" image is shown in the top right panel. The panel immediately below this one is the best fit to the "truth" image possible using the "wrong" PSF, which in this case is the PSF generated from the G5v stellar spectrum. The leftmost panel in the second row shows the above-atmosphere galaxy model used to create this "best fit" image. The rightmost panel in the third row shows the residual between the "truth" image and the "best fit" image, and is an indication of the quality of the fit in Step 5 of the ring test. If the fit were perfect, then the residual image would be entirely zeros.

The reason the residual image is not entirely filled with zeros is due to "model bias" (Voigt & Bridle 2010; Melchior et al. 2011; Bernstein 2010). The fitting step can be viewed as an attempt at deconvolution of the "truth" image by the "wrong" PSF under the assumption that the functional form of the deconvolved image is known. The best fit model (second row, first column) is the result of this attempted deconvolution, and the ellipticity parameters can then simply be read off as the parameters that generated the model. In practice, however, the true deconvolved image (i.e. the true deconvolution of the "truth" image by the "wrong" PSF) will not always be producable by the functional form of the fit. More generally, the true deconvolution may not even have elliptical isophotes, precluding a solution by simply adding degrees of freedom to the radial profile of the functional form of the model.

The degree to which the ring test results are biased by model fitting depends on how well the deconvolution is able to function. Larger residuals to the fit are more susceptible to bias. Comparing Figures 2, 3, and 4, we see visually that the residuals grow with the Sersic index, which explains how the $n = 4.0$ curve of Figure 1 became so different than the analytic prediction. All of the curves are subject to bias both model bias and bias from DCR, but the $n = 4.0$ curve is the most sensitive to model bias. Presumably, better ellipticity measurement algorithms would show less dependence on the Sersic index. For instance, the algorithms described in Bernstein (2010) and Melchior et al. (2011) both aim to mitigate model bias. If Step 5 of the ring test were replaced with one of these algorithms for measuring ellipticity, then maybe the effect of DCR could better be isolated from the effects of model bias.

REFERENCES

Bernstein, G. M. 2010, MNRAS, 406, 2793

Coleman, C. D., Bozman, W. R., & Meggers, W. F. 1960, Table of Wave numbers.

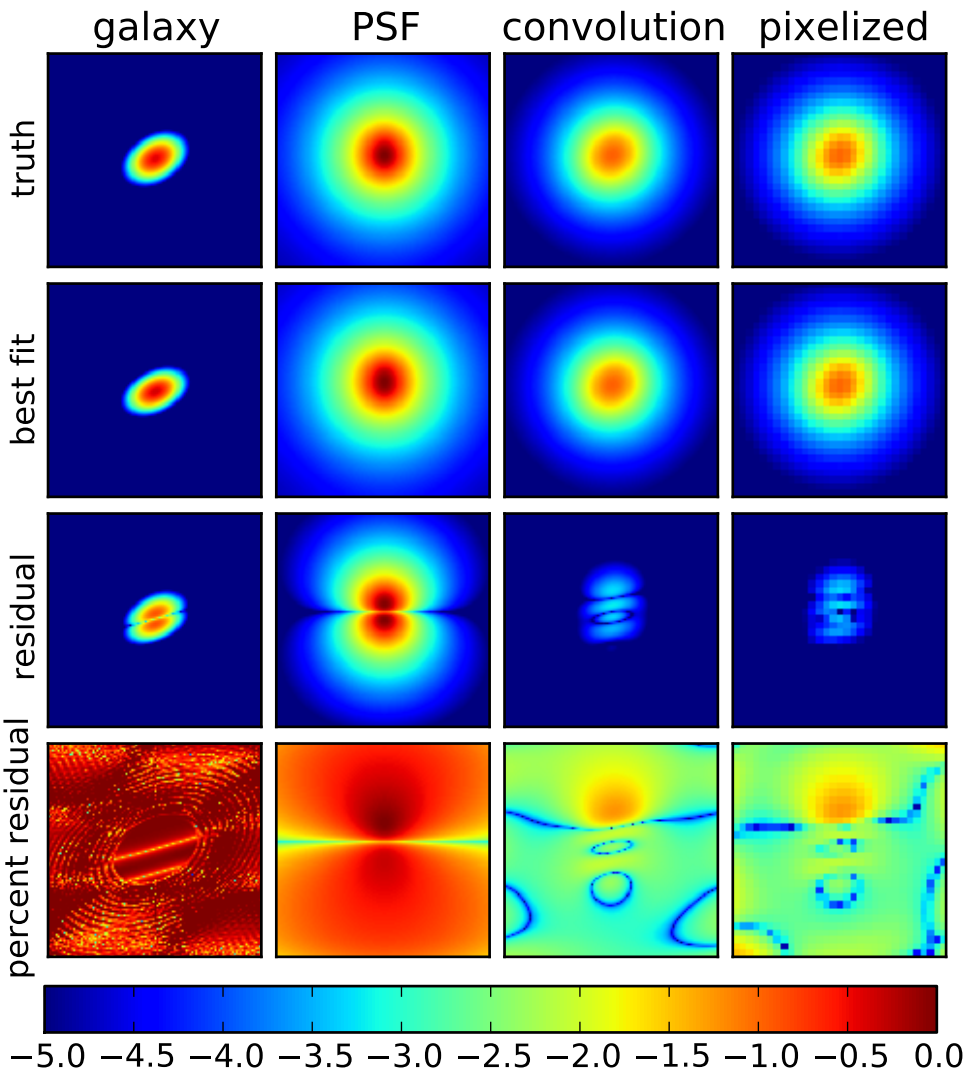

FIG. 2.— Illustration of the simulation and fitting portion of the ring test procedure (steps 4 and 5). The columns from left to right represent (i) the high-resolution model galaxy before PSF convolution, (ii) the PSF, (iii) the galaxy convolved with the PSF, and (iv) the pixelization of (iii). The rows from top to bottom represent (i) the "true" galaxy model, PSF, and convolutions, (ii) the best fit galaxy model, PSF, and convolutions, (iii) the base-10 logarithm of the absolute value of the residual ($\mathrm{bestfit} - \mathrm{truth}$), and (iv) the base-10 logarithm of the absolute fractional residual ($(\mathrm{bestfit} - \mathrm{truth})/\mathrm{truth}$). The fit is designed to minimize the pixelized residuals in the third row, fourth column. The difference between the truth and best fit galaxy models illustrates the size of the model bias induced by using the "wrong" PSF in the fit. The galaxy profile is Gaussian in this figure ($n = 0.5$, both in truth image and fixed during the fit), the galaxy PSF is derived from an elliptical spectrum at redshift 1.3, and the stellar PSF is derived from the spectrum of a G5v star. The zenith angle is 60 degrees.

Edlen, B. 1953, JOSA, 43, 339
Melchior, P., et al. 2011, MNRAS, 412, 1552
Nakajima, R. & Bernstein, G. 2007, AJ, 133, 1763
Plazas, A. A. & Bernstein, G. M. 2012, ArXiv e-prints
Voigt, L. M. & Bridle, S. L. 2010, MNRAS, 404, 458

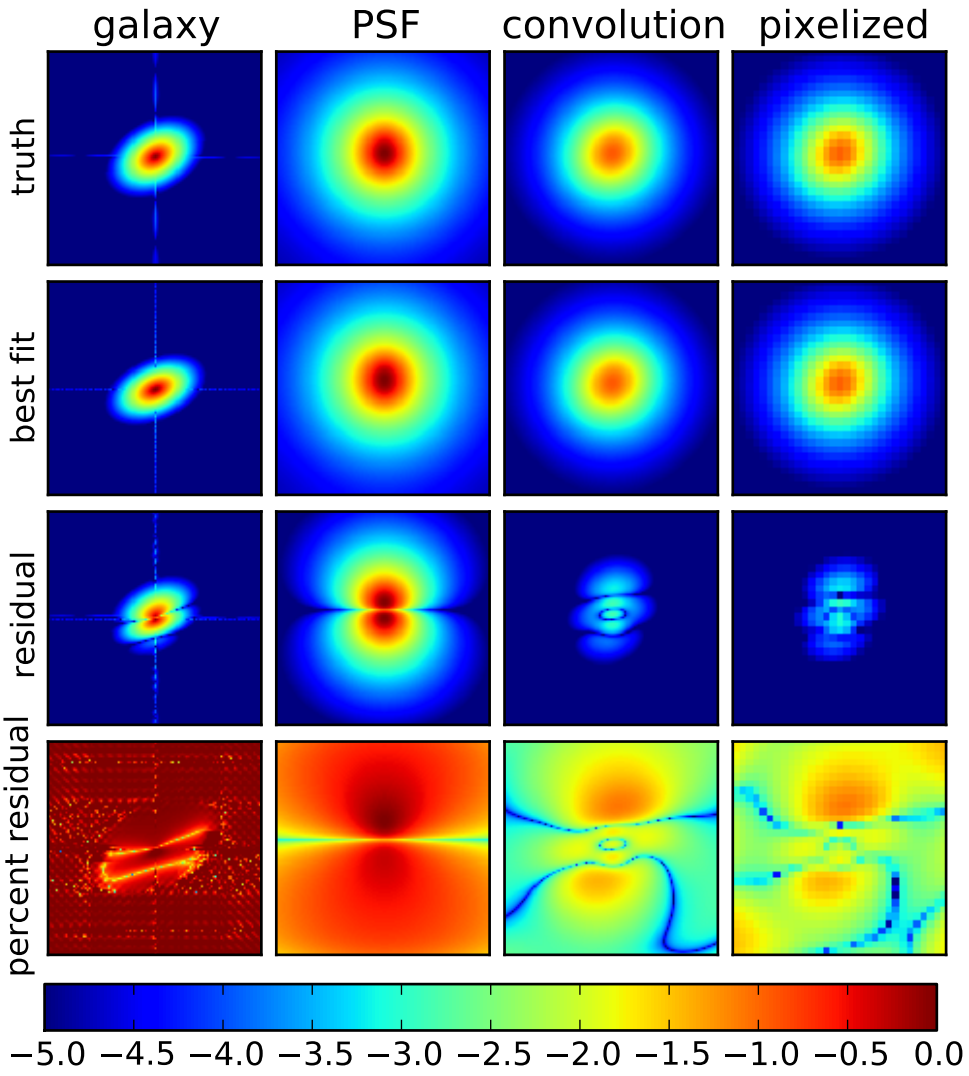

FIG. 3.— The same as Figure 2, but the galaxy profile is changed to be exponential ($n = 1.0$, in both the truth image and fixed during the fit).

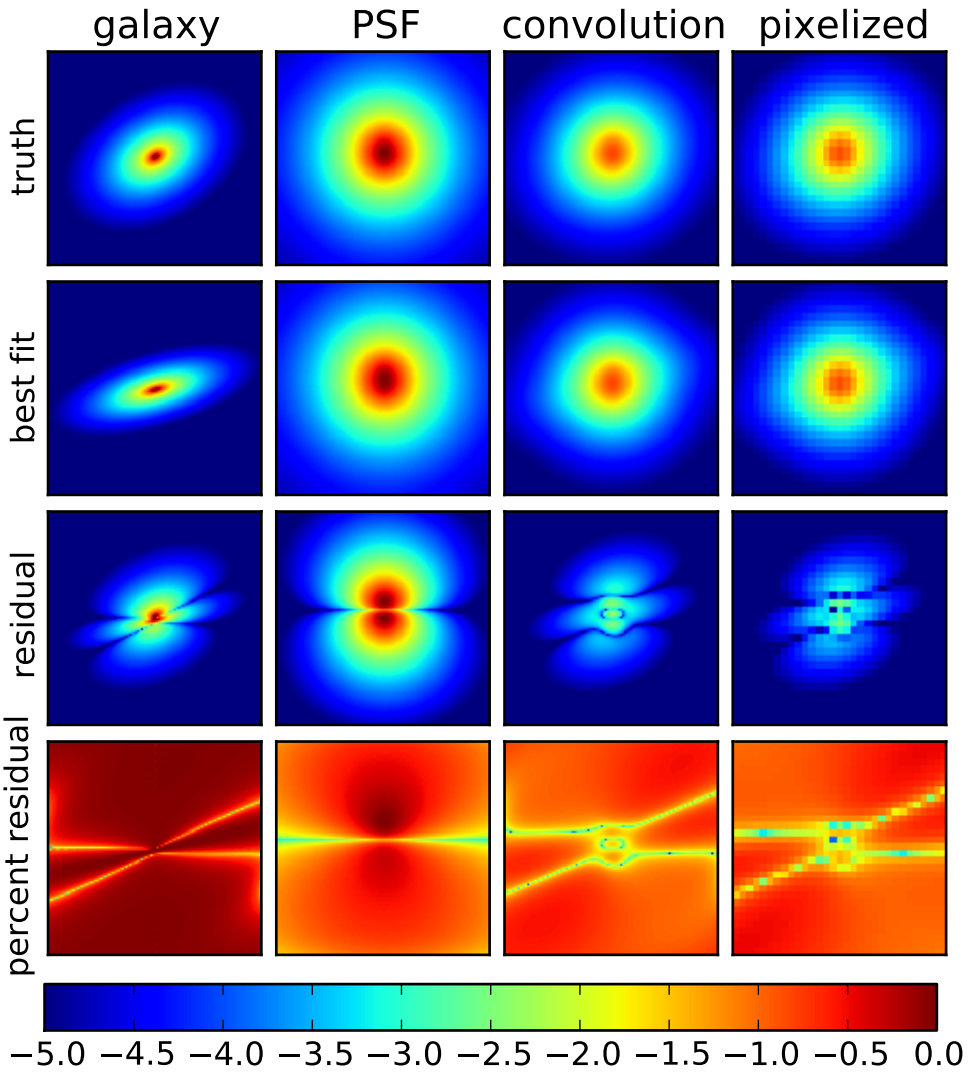

FIG. 4.— The same as Figure 2, but the galaxy profile is changed to be de Vaucouleurs ($n = 4.0$, in both the truth image and fixed during the fit).